Modeling the infilling process of an abandoned fluvial-deltaic distributary channel: An example from the Yellow River delta, China

Zhaoying Li [a], Houjie Wang [a,b,*], Jeffrey A. Nittrouer [c], Naishuang Bi [a,b], Xiao Wu [a,b], Brandee Carlson [c]

[a] College of Marine Geosciences, Key Laboratory of Submarine Geosciences and Prospecting Techniques, MOE, Ocean University of China, 238 Songling Rd., Qingdao 266100, China
[b] Laboratory for Marine Geology, Qingdao National Laboratory for Marine Science and Technology, Qingdao 266061, China
[c] Department of Earth Science, Rice University, 6100 Main Street, Houston, TX 77005, USA

ARTICLE INFO

ABSTRACT

As an inevitable result of fluvial-deltaic avulsions, abandoned distributary channels and associated lobes form an important component of coastal marine systems, serving as a sediment source and sink for the adjacent delta region. The distinct differences between normal tidal flats and abandoned channel systems restrict the application of classic intertidal mud flat morphological theory to the study of the evolution of abandoned channels. Herein, a quantitative model based on the concept of mass conservation was proposed to describe the infilling processes for an abandoned channel. Sediment cores and elevation profiles from an abandoned channel of the Yellow River delta (China), along with hydrodynamic observational data, are used to constrain a numerical approach and test model performance. The modeled accumulation thicknesses are satisfyingly consistent with those derived from sediment cores. The model results indicate that the tide-delivered sediment flux and channel water depth are the dominant variables governing the variation in accumulation thickness in the abandoned channel, whereas the channel shortening rate largely impacts the depositional area rather than depositional thickness. By contributing to steady deposition on the mud flat, tide-associated landward sediment deposition formed a steep profile near the estuary, while the final four years of deposition represent only a quarter of the total deposition compared to that from the first five years owing to a decreasing depositional rate. The model-derived sediment volume indicates that shore-parallel flow is significant in shaping mudflat morphology, especially in the late stages, while the shortening of tidal channels leads to shrinking of the mud flat and sediment volumes. Despite its limitation to residual channels, our model presents a new approach for quantitative interpretation of the geomorphic evolution of an abandoned river channel with finite boundary conditions, providing a good reference to apply to other large deltaic systems.

© 2020 Elsevier B.V. All rights reserved.

1. Introduction

River avulsion near the marine terminus is a fundamental process that controls coastal sediment deposition, forming numerous morphological patterns and environmental settings including abandoned deltaic lobes and channels (Chatanantavet et al., 2012) and occurring frequently on large rivers with high sediment flux such as the Mississippi and Yellow Rivers. By acting as sediment repositories for fluvial-marine sediments, abandoned deltaic channels are important to the development of coastal morphology. Sediment deposits in these settings record hydrodynamic variations such as tides and waves. Various publications have focused on delta lobe erosion after fluvial abandonment (Frazier, 1967; Penland et al., 1988; Wang et al., 2006; Nienhuis et al.,

2013; Zhou et al., 2014), but the depositional processes within abandoned channels rarely have been examined (Carlson et al., 2020).

Upon losing a direct water-sediment supply from the main river, the hydrodynamical environment of an abandoned deltaic channel is primarily influenced by tides and waves, often leading to the evolution of a tidal flat (Carlson et al., 2020). Within the intertidal zone, the linkage between subaerial and submarine environments is a significant component of coastal and estuarine systems; these environments are characterized by a shallow gradient and are therefore susceptible to repeated inundations that impact sediment dynamics. Over the last few decades, tidal flat morphology has been studied extensively, and several numerical models for the evolution of intertidal landforms have been proposed. Friedrichs and Aubrey (1996) advanced a theory of intertidal flat morphology (referred to herein as "FA96"). According to FA96, the maximum tidal velocity is assumed to be stable in subtidal and lower flat regions and to decrease in the upper flat with distance from the low water line. This provides a useful analytical model for summarizing morphodynamical processes. More recently, multiple mechanisms have

* Corresponding author at: College of Marine Geosciences, Key Laboratory of Submarine Geosciences and Prospecting Techniques, MOE, Ocean University of China, 238 Songling Rd., Qingdao 266100, China.
  E-mail address: hjwang@mail.ouc.edu.cn (H. Wang).

(a)

(I)

(II)

(b)
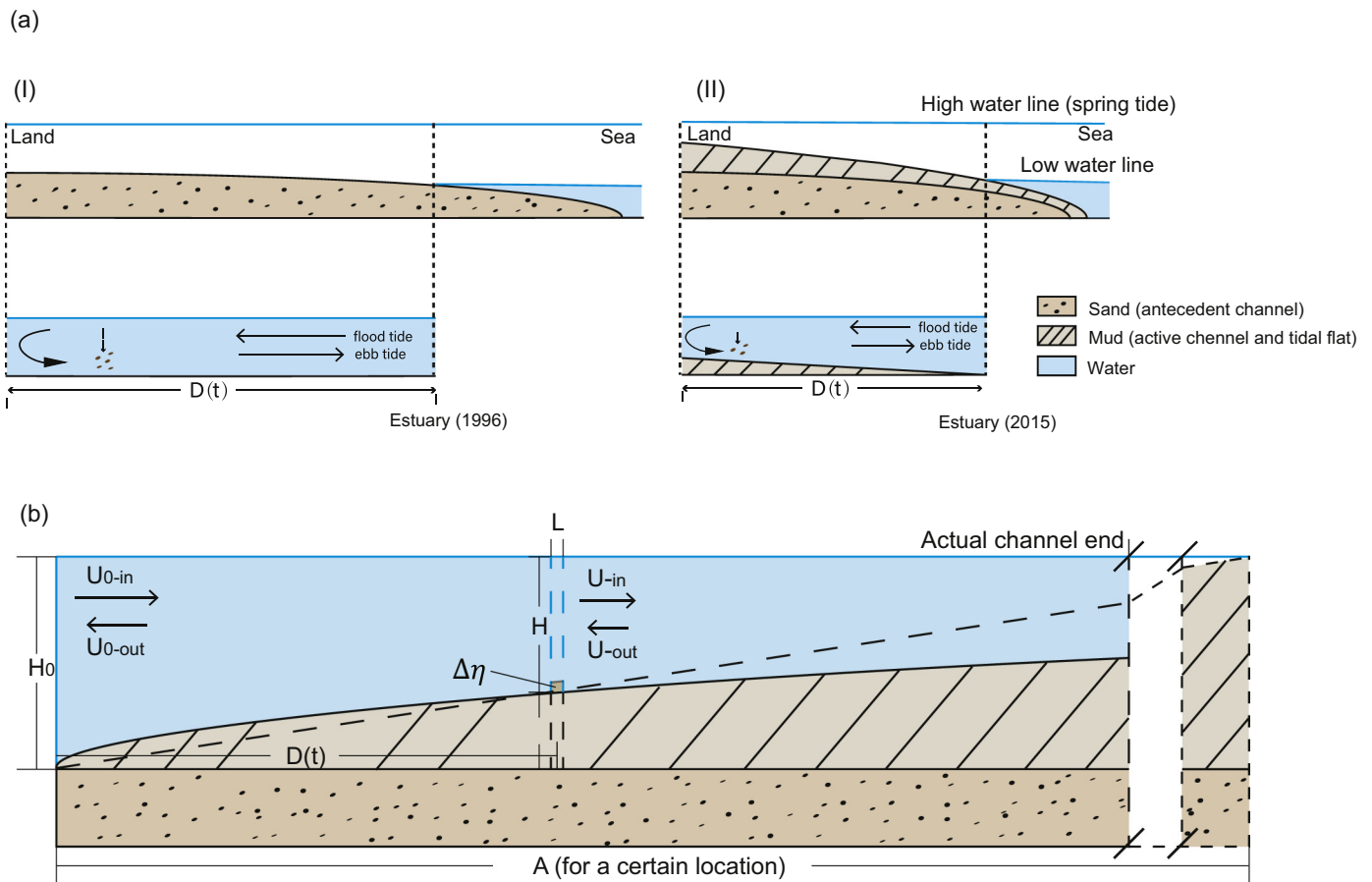
Fig. 1. a) Schematic view of an abandoned channel (not to scale): (I) channel profile at the beginning of abandonment with tidal conditions; (II) channel profile after abandonment with evident lobe shortening, in-channel mud deposition, and correspondingly changing tidal conditions; and b) schematic diagram of in-channel deposition over a tidal cycle (not to scale). The symbols are listed in Table 1.

been suggested to describe the sedimentation over tidal flats to shape the shore-normal profile (Lee and Mehta, 1997; Le Hir et al., 2000; Roberts et al., 2000; Pritchard et al., 2002; H. J. Lee et al., 2004;). The core concept of muddy profile progradation is primarily derived from mass conservation, yielding a dynamic equilibrium theory (DET) proposed by Friedrichs (2011) with spatial and local asymmetries (Hsu et al., 2013; Hu et al., 2015; Hu et al., 2018). Mariotti and Fagherazzi (2010) developed a comprehensive numerical model for long-term evolution of salt marshes and tidal flats and discussed the morphological evolution of tidal channels and unvegetated tidal flats (Mariotti and Fagherazzi, 2013). Xu et al. (2019) investigated a two-dimensional model for the development of tidal channels using flow and sedimentation models. Vegetation and ecogeomorphic factors significantly influence tidal flat and tidal channel evolution (Fagherazzi et al., 2012; Belliard et al., 2015; Kearney and Fagherazzi, 2016).

These classical models have several limitations when applied to the evaluation of the morphological development of an abandoned deltaic channel. First, abandoned channels, especially those in mud flats (the object of study here), are complex sedimentary environments that are very different from the classic tidal flat. Compared with an open and broad coastal zone tidal flat, tide water intrusion into an abandoned channel is restricted by identifiable levees from the antecedent river channel, which affects the hydrodynamic environment. Concurrently, an abandoned channel maintains a morphological structure that is highly variable, inheriting the form of the previously active channel, and thus can differ from a traditional tidal channel formed by ocean dynamics. For example, channel depth is initially set by the antecedent bed before abandonment, and as the estuary develops, this morphology naturally changes as

a consequence of sediment deposition and erosion (Carlson et al., 2020). In turn, this produces a feedback effect on the maximum/minimum flood and ebb water surface elevations (respectively). Second, classical tidal flat models are developed based on the hypothesis that sediment is transported exclusively by periodic tides and waves and deposited on a relatively flat surface (Friedrichs, 2011), and thus the flat is a net sediment sink. While an abandoned lobe may behave similarly, it can also be eroded as sediment is recycled and transported landward before deposition on a flat. Thus, the sediment sources for abandoned channels are nonunique. A new approach is therefore required to model this dynamic in-filling regime for an abandoned deltaic channel while preserving sediment mass conservation.

This study establishes a quantitative model to describe sediment depositional processes and morphological development associated with the infilling processes of an abandoned fluvial-deltaic channel, with the core concepts of the model grounded in mass conservation. In-situ observational data collected from an abandoned distributary channel of the Yellow River delta (China) are used to constrain a filling model and test its accuracy when using different boundary conditions to explore the model sensitivity. Additionally, sediment deposition rates and infilling volume are evaluated by analysis of sediment samples, and the model results are inverted to constrain filling processes from 1996 to 2015.

2. Model description

The establishment of a depositional model with appropriate boundary conditions describing the environmental situation is required.

3

According to previous work (Carlson et al., 2020), the abandoned channel is influenced by sedimentation resulting from tide-induced overbank deposition, which is especially enhanced under spring tide conditions. This creates a gentle channel-normal slope as sediment accumulates over time onto the adjacent tidal channel. Additionally, the tidal channel possesses a shore-normal slope constructed by continued deposition due to tidal processes. We explore both of these slopes in detail below and define an abandoned channel infilling model, while boundary conditions and observational data from Yellow River delta have been used to test the model robustness.

2.1. Shore-normal slope (slope 1)

The development of a graded tidal channel slope is affected by a combination of factors, including tidal amplitude, discharge, sediment concentration, and current velocity. As the abandoned channel was not immediately submerged but instead was exposed at low tide and inundated with sediment-laden water during periodic high tides, sediment deposited within the channel eventually transformed the surface into a typical mud flat. When the initial avulsion occurs ($t = 0$), the newly abandoned channel begins to aggrade, generating a mudflat with a relatively flat surface (Fig. 1a) as energetic flood tides inundate the bed and deposit sediments during slack tide periods. Tidal asymmetry produces a lag deposit (Straaten and Kuenen, 1958; Postma, 1961), and over time, the deposit thickness increases. Importantly, this influences the bed slope, which in turn affects current velocity, producing feedback affecting the sediment deposition rate (Fig. 1a). Simultaneously, continued erosion of the lobe front effectively shortens the subaqueous channel.

For analysis of depositional processes within the abandoned channel, a time period over one tidal cycle is assessed. The parameters used for analysis and their physical meanings are shown in Table 1. Fig. 1b illustrates sediment deposition at a given location over a tidal cycle (Δt). $D(t)$ is used to represent the average distance from the estuary, and L represents the length scale over which sedimentation occurs. It is assumed that water depth and velocity exiting the estuary are constant and are labeled H_0 and U_0, respectively. Therefore, the water depth (H) at a given location is expressed as the difference between H_0 and local bed elevation η (sediment deposition). The depositional thickness $\Delta\eta$ varies with time over a tidal cycle.

According to the concept of mass conservation, the water depth as a function of time is equal to the sediment flux change at a given location over a tidal cycle:

$$\frac{dH_0(t_1)}{dt_1} + \frac{\partial}{\partial D}\{(H_0-\eta)\cdot U\} = 0 \tag{1}$$

where current velocity is given as:

$$U = \frac{A-D}{H_0-\eta}\cdot\frac{dH_0(t_1)}{dt_1} = \frac{A-D}{H_0-\eta}\cdot H_0'(t_1) \tag{2}$$

Table 1
Description of model parameters.

Symbol	Name	Unit	Symbol	Name	Unit
V	Sediment volume	m³	η	Sediment thickness	m
Q_s	Sediment flux	m³/s	L	Length of water body	m
e	Erosion rate	m/s	λ_p	Porosity	/
U	Current speed	m/s	S	Channel slope	/
C_m	Sediment concentration	kg/m³	H	Water depth	m
ρ	Sediment density	kg/m³	B	Width of channel	m
D	Distance to estuary	m	m	Original distance	m
n	Distance to tidal channel	m	t	Time	s

The unknown parameter, A, is the distance from the low to the high water line for a tidal flat with a slope S (Friedrichs and Aubrey, 1996). However, the length of the abandoned channel body is not enough for the tide to reach its high-water line because of the limited remaining channel body. A is a parameter that determines where sedimentation occurs (Fig. 1b) and is calculated as the quotient of the water depth in the estuary and the along-channel slope:

$$A = \frac{H_{0-max}}{S} = \frac{H_{0-max}}{\eta}\cdot D \tag{3}$$

Substituting A into Eq. (2) yields a result between U and U_0 with another unknown parameter, a.

$$U = \frac{D}{\eta}\cdot\frac{H_{0-max}-\eta}{H_0-\eta}\cdot H_0'(t_1) = \frac{D}{\eta}\cdot\frac{\eta_0}{D_0}\cdot U_0 = a\cdot\frac{D}{\eta}\cdot U_0 \tag{4}$$

The deposition elevation variation ($\Delta\eta$) is equal to the sediment volume carried and deposited during a tidal cycle (Δt). Considering the bulk density and porosity of sediment, the balance on both sides of the equation yields:

$$V = Q_s\cdot\Delta t = B\cdot H\cdot(U\cdot C_{m-in}-U\cdot C_{m-out})\cdot\frac{1}{\rho}\cdot\Delta t = \Delta\eta\cdot L\cdot B\cdot(1-\lambda_p) \tag{5}$$

At a given location, the distance (D) is expressed as a function controlled by the shoreline retreat rate of the abandoned lobe, original distance, and time:

$$D = D(t) = m-et \tag{6}$$

Calculating D, for which the water depth is the difference between H_0 and η,

$$\frac{\Delta\eta}{\Delta t} = \frac{a}{L\cdot\rho\cdot(1-\lambda_p)}\cdot(H_0-\eta)\cdot\Delta UC_m\cdot\frac{m-et}{\eta} \tag{7}$$

yields the relationship between depositional thickness, time, and location.

$$a\cdot\frac{1}{L\cdot\rho\cdot(1-\lambda_p)}\cdot\Delta UC_m\left(-\frac{1}{2}et^2 + mt\right) = -\eta-H_0\cdot\ln\frac{|H_0-\eta|}{H_0} \tag{8}$$

Eq. (8) expresses the variation of depositional thickness with time.

2.2. Shore-parallel slope (slope 2)

Under normal circumstances, after an avulsion, the abandoned channel would be accessed by tides and be subject to sedimentation as described above. In spring tide conditions, when rising tidal currents cover the entire channel (Fig. 2a), sediment-laden water flows from outside the confines of the tidal channel onto the mudflat (Carlson et al., 2020). The process of tidal flow being maximized by a spring tide and spreading over a mudflat is termed "overbank" below. The overbank deposit forms a relatively thick deposit over time, as shown schematically in Fig. 2b and herein termed a "levee". Note that deposition near the tidal channel is relatively flat and not tapered as found in the actual river channel levee. Here, this "levee" is considered as a boundary between the tidal channel and the mudflat.

Unfortunately, there are no numerical schemes that can be used to describe levee depositional processes and morphological evolution over time due to uncertainties such as the spatial heterogeneity of channel hydrodynamics. However, sediment distribution from field data can be used to approximate sediment depositional patterns occurring since channel abandonment. Here, elevation and sediment core data collected in the Qingshuigou distributary channel of the Yellow River delta
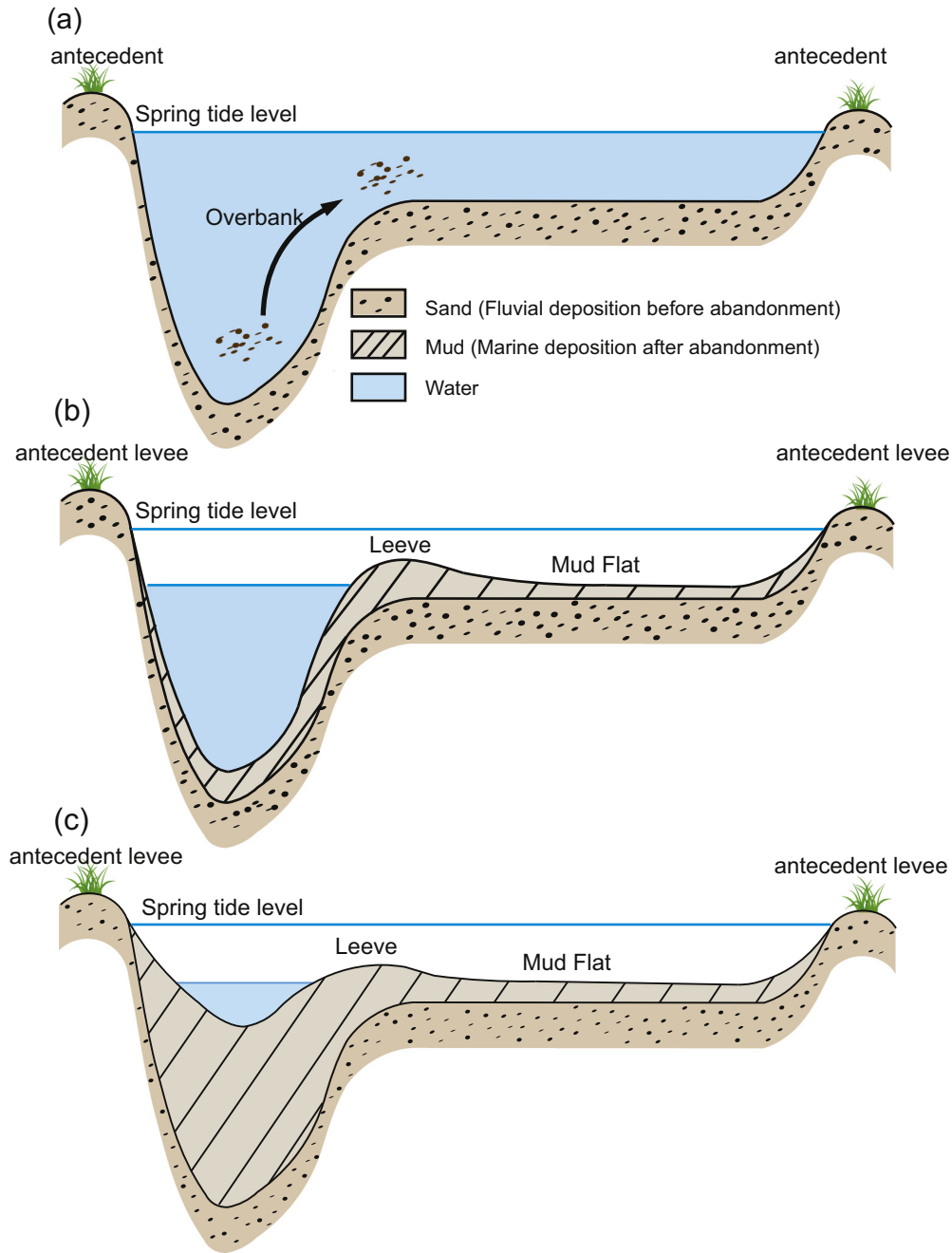
Fig. 2. Schematic diagram of a sectional profile of an abandoned channel (not to scale) showing its evolution in different stages: a) immediately after abandonment; b) the middle stage when overbank deposition leads to the formation of a mudflat; and c) the final stage with infilling of mud over the previous fluvial sand deposition.

(abandoned in 1996) are used as an example to constrain mudflat sediment thickness (see Carlson et al., 2020; Wu et al., 2020) (Figs. 3 and 4). The data demonstrating a depositional maximum at approximately 80–100 m from the tidal channel and a gradual seaward decrease approximately follow a natural logarithmic function (Fig. 3).

This depositional pattern produces slope 2, expressed for a given location by:

$$\eta = r \cdot t = \frac{p_1 \cdot \ln n + p_2}{t_{19}} \cdot t \qquad (9)$$

where r is the deposition rate and t is time. Assuming that r is constant for the 19 years since abandonment (1996–2015), the deposition rate at a given location (n, representing distance to tidal channel) can be calculated. In Eq. (9), p_1 and p_2 are unknown parameters that can be assessed

empirically. A similar tendency can be used as a reference in normal abandoned channels to assess the common influence of tidal channels.

2.3. Model verification

Deposition in an abandoned channel can be described as a composite of processes arising due to tidal channel and overbank sedimentation. The model can be written:

$$\eta = \eta_1 + \eta_2 \qquad (10)$$

where η_1 is deposition forming slope 1 (shore-normal slope) and η_2 is deposition forming slope 2 (shore-parallel slope); however, there is no evidence to establish which slope contributes more to the final result, implying that a parameter is needed to quantify the effects of
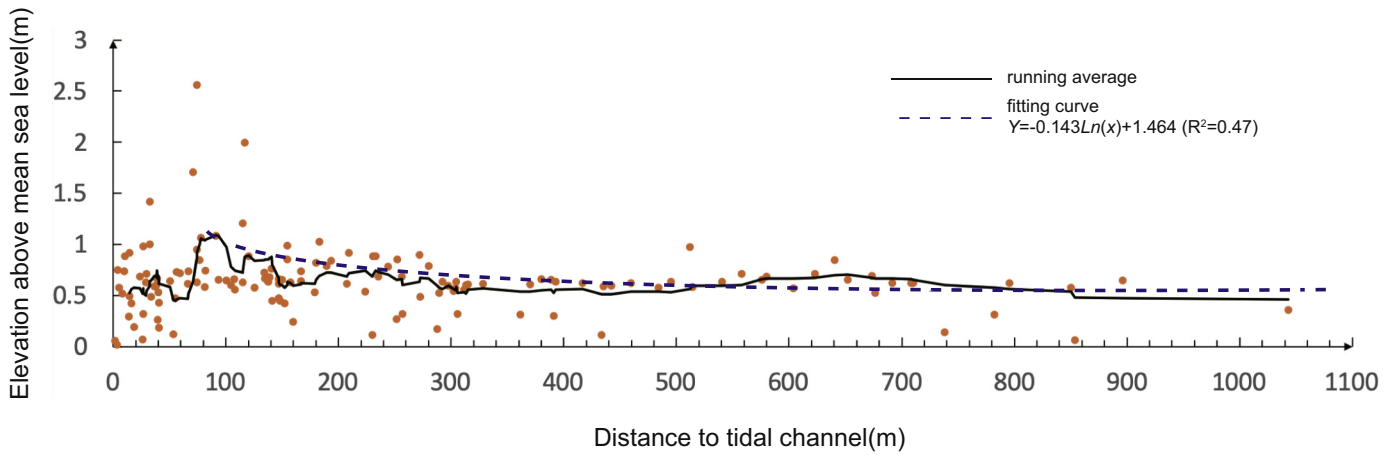
Fig. 3. Elevation data for the modern mud flat surface in the Qingshuigou abandoned distributary channel, of the Yellow River delta, referenced by distance from the tidal channel to the sea. Black line is the running average and the dashed line is the fitting curve using a natural logarithmic function.

different factors. Here, i is used to evaluate the level of influence with a range of 0–1, defined as:

$$i = \frac{\eta_1}{\eta} \qquad (11)$$

A higher value for i indicates a stronger influence attributable to slope 1 (tide), and conversely, a lower i indicates a stronger influence attributable to slope 2.

We used this model to investigate a recently abandoned river channel in the Yellow River delta (Fig. 4). The Qingshuigou channel extended southeastward and was abandoned in May 1996 due to an artificial channel shift (Fig. 4b). After its abandonment, tide-induced landward transport of sediment accumulated in the Qingshuigou distributary channel. To understand how these hydrodynamic characteristics influence the abandoned channel, a field survey was conducted in the Laizhou Bay adjacent to the mouth of the Yellow River in August 2003. The resulting data allowed us to estimate landward transport into the

abandoned Qingshuigou channel over a tidal cycle (see Bi et al., 2010). At a station located near the Qingshuigou mouth, current meters were used to synchronously and continuously record flow speed and current direction in the surface, middle and bottom layers of the water column. Sediment concentration was also measured and combined with current velocity data to estimate the flux of both water and sediment. Sediment fluxes during the flood and ebb tides were estimated to be 2.90×10^{-2} kg/s · m^2 and 2.72×10^{-2} kg/s · m^2, respectively, yielding a net sediment delivery to the abandoned channel over a tidal cycle of 1.79×10^{-3} kg/s · m^2 (Bi et al., 2010).

Parameter ρ represents the bulk density of sediment particles, which is estimated to be 2650 kg/m^3, and the sediment porosity, λ_p, is approximated as 0.415 for sediments in the tidal flats of the Yellow River delta (Jia and Shan, 2011). The initial water depth, H_0 (see Fig. 1b), of the bankfull flow depth of the Yellow River at the beginning of abandonment is set at 3 m by using previous in-channel observations (Wang et al., 2007). After the channel abandonment in 1996, severe coastal erosion led to a shortening of the abandoned channel (Fig. 5). Based on
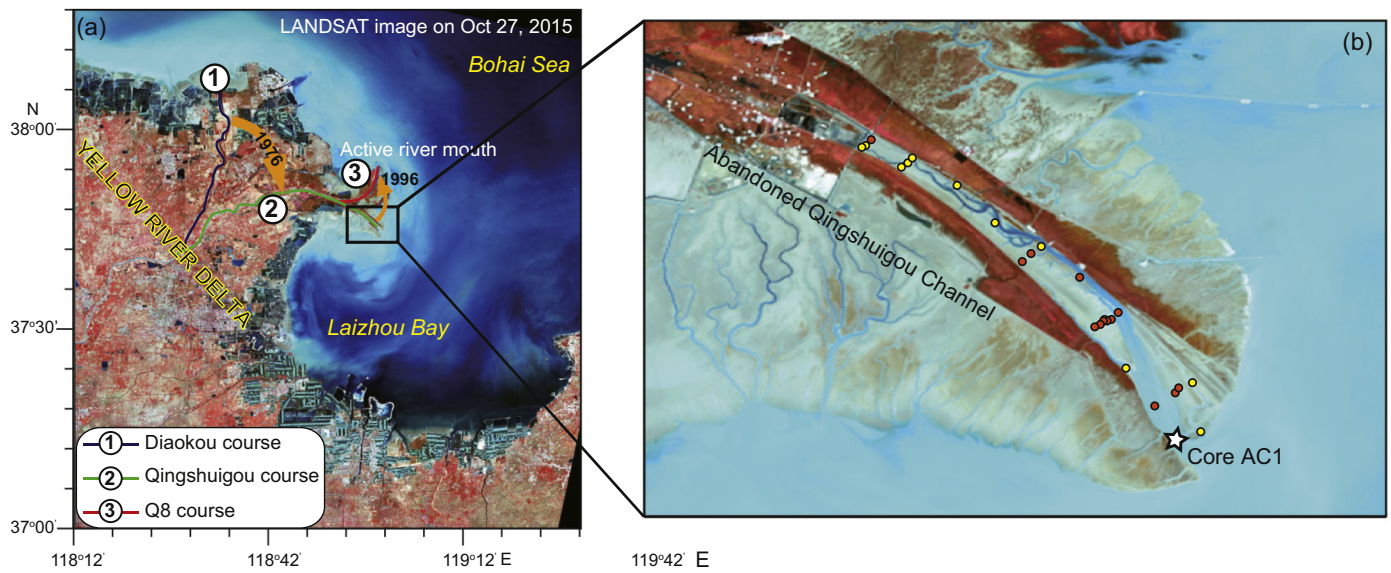
Fig. 4. a) LANDSAT image of the modern Yellow River delta illustrating recent shifts of the lower river courses; b) the Qingshuigou distributary channel abandoned after 1996. Dots indicate locations of 14 vibracores (yellow) and 13 pits excavated in the channel (red), and the location of Core AC1 (white star) for sedimentary analysis (Carlson et al., 2020; Wu et al., 2020).
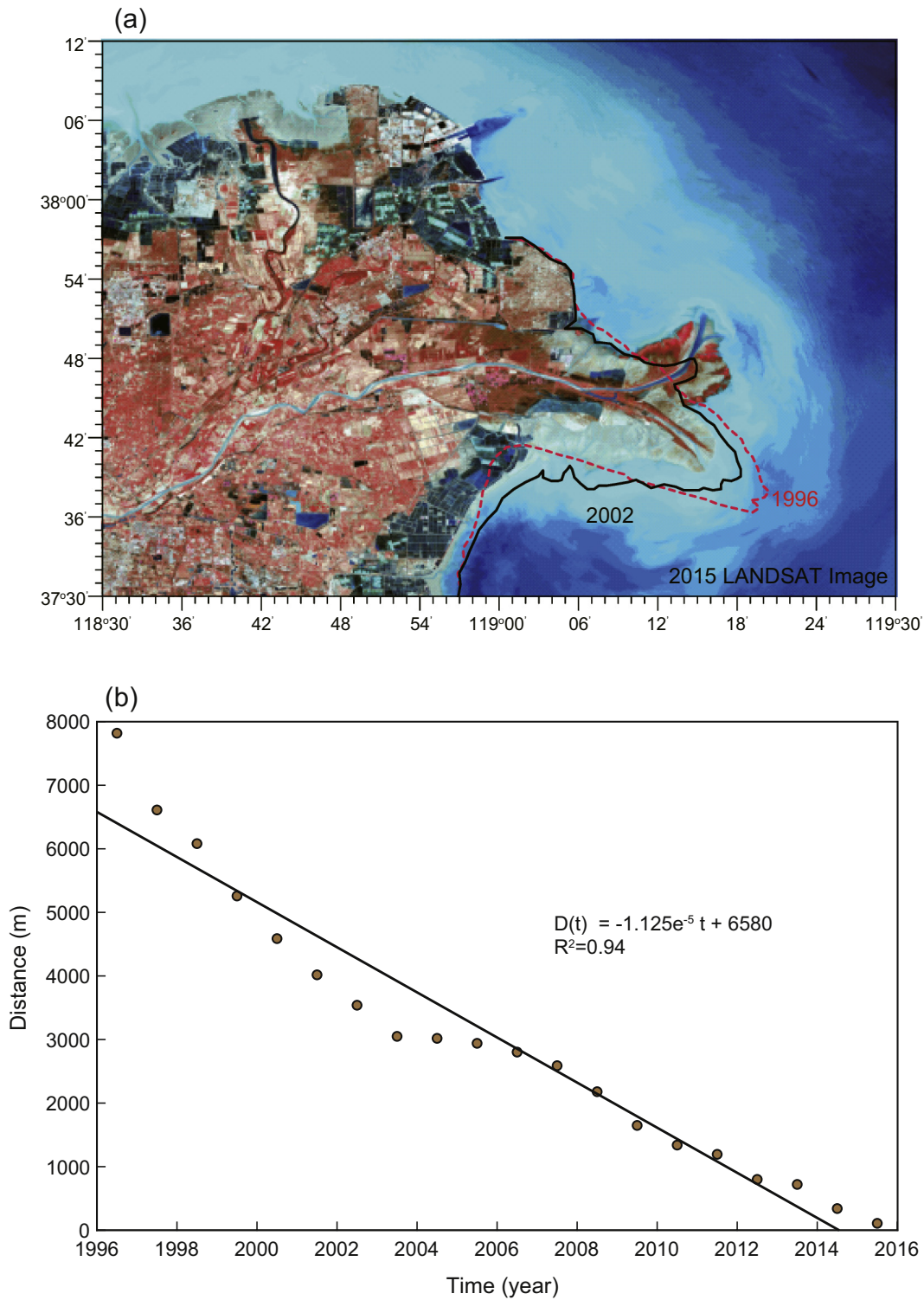
Fig. 5. a) Coastlines of the active delta lobe from 1996 to 2015, extracted from LANDSAT images in 1996, 2002 and 2015; b) annual variation in distance (or channel length) from 1996 to 2016. Black line indicates a fitting curve.

LANDSAT images (1996–2015), the annual average value of D was estimated (Fig. 5b), yielding a significant regression ($R^2 = 0.94$) of parameter D as a function of time t as follows:

$$D(t) = -1.125 \times e^{-5} t + 6580 \qquad (12)$$

The channel length seemed to be relatively stable for a short period (2004–2006), which was perhaps due to the increasing sediment load from the Yellow River resulting from the implementation of the Water-Sediment Regulation Scheme (Wang et al., 2017), which intermittently slowed erosion but did not essentially change the decrease in channel length (Fig. 5b).

Based on the average boundary condition values (see Table 2), the accuracy of the model is tested using observational data from the Qingshuigou abandoned channel. The data from sediment cores collected in the abandoned channel are categorized into two groups: the

Table 2
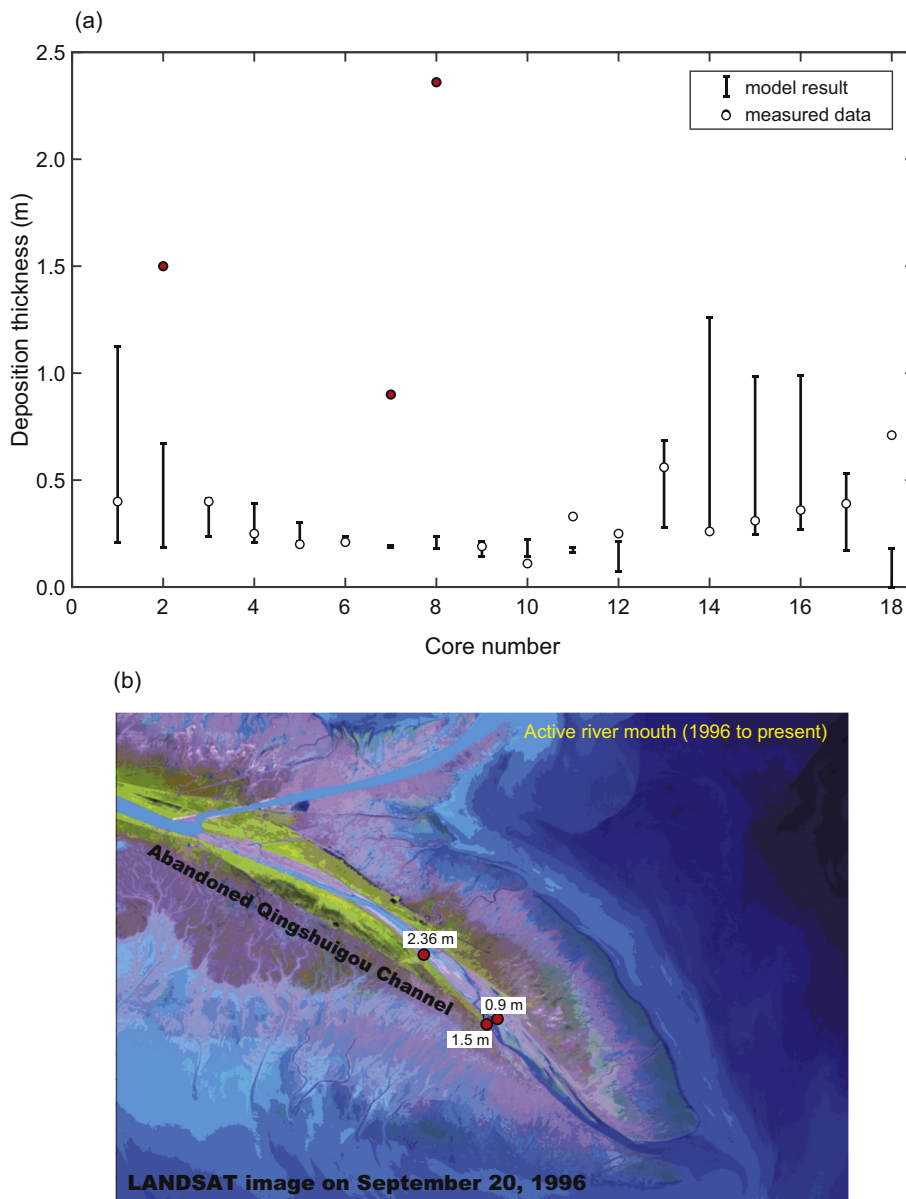Boundary conditions for model application.

Symbol	Name	Value	Unit	Data resource
λ_p	Porosity	0.415	/	Jia and Shan, 2011
ρ	Sediment density	2650	kg/m^3	/
$Q_{s-mass1}$	Net sediment flux (summer)	1.79×10^{-3}	kg/s · m^2	Bi et al., 2010
$Q_{s-mass2}$	Net sediment flux (winter)	3.58×10^{-2}	kg/s · m^2	Wang et al., 2016
D_0	Original distance to estuary	6580	m	LANDSAT images
H_0	initial water depth	3	m	Wang et al., 2007

calculated portion (containing 9 cores) and the test portion (containing 18 cores). The calculated portion was used to determine unknown parameters in the model, including a, p_1, and p_2, with different i values. The parameters were then applied to test the model results by comparing the model output with data from the test portion (Fig. 6a). The range of model results are represented with different i values and the corresponding p_1, p_2, and median a values. These analyses indicate a result that is relatively consistent with the test data, as most points fall within the model range, indicating that the model could be used to estimate sediment depositional thicknesses within the abandoned channel.

There are three cores with extremely high depositional thickness that exceed the model range (Fig. 6a). This might be explained by the proximity of these sampling locations to the channel thalweg. The LANDSAT imagery acquired on September 20, 1996 (weeks after the engineered avulsion, Fig. 6b) indicated that portions of the Qingshuigou distributary channel were natural topographic lows as a consequence of the position of the thalweg, and the areas of high recorded mud thickness were located within these areas (Carlson et al., 2020).

Since we have a range of values from which we can inform the model, it is useful to explore the optimal values for the unknown

Fig. 6. a) Comparison between the modeled depositional thickness and those derived from sediment cores collected in 2015 (core locations shown in Fig. 4b). Black lines indicate model value ranges based on varying boundary conditions. Red dots indicate cores with extremely high depositional thickness. b) Locations of sediment cores with extremely high depositional thickness on a LANDSAT image (September 20, 1996), indicating that abnormal highs are likely correlated with the proximity of core locations to the channel thalweg.

parameters. Each i had an exclusive group of a, p_1, and p_2 values obtainable by calculation. The parameter ranges are compared with the test portion in Fig. 7, where parameter i is a dimensionless index defined by Eq. (11) indicating the contribution of slope 1 that maintains a value between 0 and 1. In other words, a higher i value indicates a greater contribution from spring tides. To highlight this influence, we tested i using values of 0.2, 0.5 and 0.8. A value of $i = 0.2$ means that overbank processes are the main depositional influence, while $i = 0.8$ indicates a greater influence of the tidal channel on the depositional process. We found that $i = 0.8$ produced the best fit with the measured data, mostly around the 1:1 line (Fig. 7), corresponding to parameter values of $p_1 = -0.087$, $p_2 = 0.584$ and $a = 2.55 \times 10^{-10}$.

2.4. Model caveat

It is acknowledged that model performance relies upon ideal conditions, and tolerances must be analyzed. First, in the model construction, it is assumed that the abandoned channel possesses a flat surface; however, given the topographic complexity of channel beds, an undulating surface can be expected, and this might be a source of error in the model. Despite this, model outcomes derived by assuming a flat slope may not deviate too far from reality. While the Yellow River channel bed is expected to have some along-stream slope in its final reaches, the value is likely minimal. Additionally, the bedform topography of the Yellow River is quite subtle, with dune aspect ratios ten times greater than those found in other sand-bed river channels (Ma et al., 2017), implying that bedform features are not a controlling factor in local elevation variability.

Second, there is an implicit assumption that sediment is not remobilized after deposition. When modeling the depositional processes of the Qingshuigou lobe, the possible movement of sediment is not incorporated, mainly because these unexpected events cannot be well-constrained using field observations. The Bohai Sea maintains seasonal variations in terms of and dynamics and sediment concentration (Wang et al., 2014); thus, landward transport of sediments into the abandoned channel is likely to vary seasonally. For the Yellow River delta, winter storms may considerably change the landform and cause significant coastal erosion (Yang et al., 2011), which can remove sediment accumulation on mud flats and accelerate the shortening of channels. According to observational data near the mouth (37.762°N, 119.400°E) obtained in January 2016, sediment concentrations were 18–28 times greater than those in summer; therefore, when performing model calculations, winter sediment flux into the abandoned channel can be assumed to be up to twenty times higher than that observed in summer conditions.
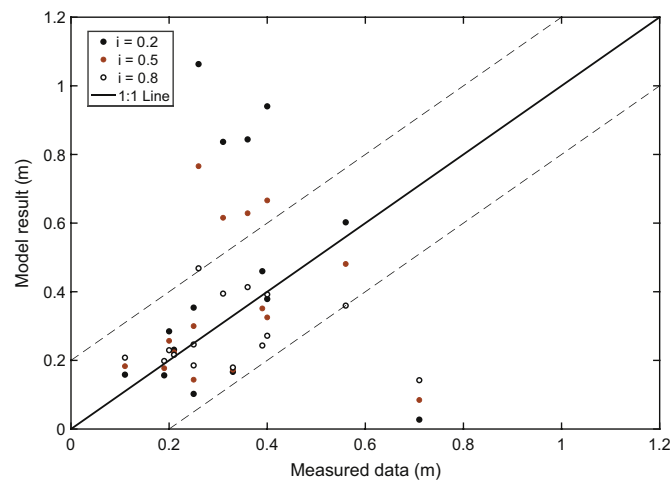
Finally, the model does not include the dynamic behavior of the mud flat surface. For example, to estimate slope 2, the channel profile illustrated in Fig. 2 is used, assuming a mud flat location that does not shift with time. However, the antecedent channel is buried in sediment (Fig. 2b and c; Carlson et al., 2020). In this situation, the tidal channel can become shallow and narrow with time, leading to expansion of the mud flat and resulting in occasional cores with extremely high values (Fig. 6). This could cause enhanced depositional thicknesses and, moreover, cannot be described by the equation for slope 2 (overbank).

3. Data and materials
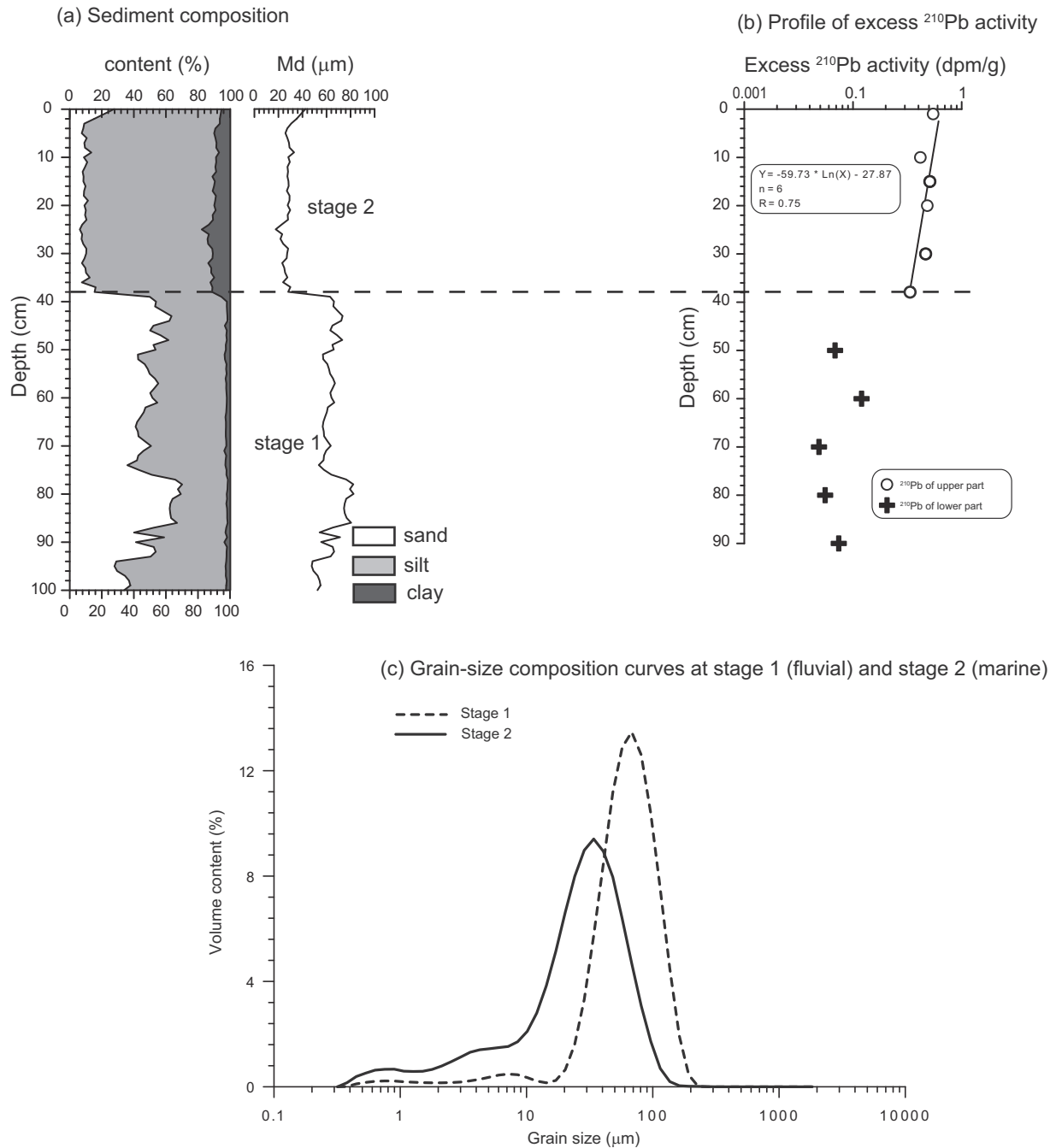
3.1. Study area and data source

As the second largest river in the world, with sediment load maximums of up to 1.08×10^9 tons per year (Milliman and Meade, 1983; Milliman and Syvitski, 1992), the Yellow River is regarded as an excellent natural laboratory for investigating the healing processes of abandoned channels. Frequent channel avulsions (approximately once every decade) and the resulting lobate landforms built by each event comprise the modern Yellow River delta complex (Pang and Si, 1979; Wang et al., 2006; Xue, 1993). The high number of abandoned channels and deltaic lobes provide a good setting to test an integral variation model over a relatively short time.

In 1976, the lower Yellow River shifted from the Diaokou course to the Qingshuigou course (Fig. 5a) with the southeastward migration of the deltaic depocenter. In May 1996, with the Yellow River deltaic mainstream artificially diverted to the present Q8 course (Fig. 5a), the Qingshuigou delta lobe was then abandoned and eroded, entering into a distinctly destructive phase resulting from cutoff of the fluvial sediment supply and continuous erosion by tidal and wave dynamics (Wang et al., 2006). However, an abundance of suspended sediment from the outer estuary (sourced from the adjacent nearshore region) along with sediments that eroded from the lobe provided a sediment source to initiate infilling of the abandoned fluvial channel. As a result, the Qingshuigou distributary channel is characterized by recent abandonment, an energetic environment with strong wave and tidal dynamics, and a considerable sediment supply. Furthermore, this abandoned deltaic lobe has been the subject of numerous recently completed investigations that collectively provide detailed sedimentological and hydrodynamic data, making it a favorable site for testing models of channel infilling processes. Specifically, for this study, analysis of sediment cores within the abandoned channel are utilized to constrain our model (Carlson et al., 2020; Wu et al., 2020). The core dataset collected from the Qingshuigou abandoned fluvial channel includes 36 samples with lengths of approximately 4 m and has been utilized for model verification.

3.2. Sedimentary environment

To analyze the depositional environment, we utilize sediment grain-size, composition, and lead isotope (^{210}Pb) dating from a typical core (AC1) with a length of 100 cm located at the outlet of the Qingshuigou course (37°40′4 N, 119°15′4E) (Fig. 4b). The primary grain-size parameters and excess ^{210}Pb dating were presented in a previous study (Fig. 8; Wu et al., 2020).

The AC1 core can be divided into two segments characterized by different sedimentary features and lead isotope results (Fig. 8a and b). The upper segment (0–38 cm) contains moist yellowish-gray silty-clay sediments without clear stratification mingled with iron nodules. Moist khaki, fine silt and silt-sand, with black stripes containing heavy mineral grains, constitute the lower segment (38–100 cm). Using the sedimentation and grain-size parameters of Core AC1, it was divided into stage 1 (100–38 cm) and stage 2 (38–0 cm) with a varying spectrum of grain-size distribution (Fig. 8c). A unimodal distribution with a maximum

Fig. 7. Comparison between core data and model results using different i-values. Each i-value corresponds to an a-value and a p-value.

(a) Sediment composition

(b) Profile of excess ^{210}Pb activity

(c) Grain-size composition curves at stage 1 (fluvial) and stage 2 (marine)

Fig. 8. a) Sediment composition and grain-size analysis for Core AC1, collected in 2015 (locations shown in Fig. 4b); b) excess ^{210}Pb profile for Core AC1; and c) grain-size distribution of samples collected from Core AC1 (after Wu et al., 2020).

volume but a minimal accompanying fine component was found in stage 1, suggesting a relatively energetic sedimentary environment. The maximum-percentage grain size of a unimodal distribution curve in stage 2 is 30 μm, and the rapidly increasing percentage of fine-grained sediments is diagnostic of a sedimentary environment differing greatly from that of stage 1. The large increase in clay content (10.3%) and abrupt decrease in sand content (10.25%; Fig. 8a) may be indicative of an evident change in sedimentary environment. Consequently, Core AC1 presents two unique depositional conditions: the upper segment (0–38 cm) has features suggesting calm conditions, while the lower segment (38–100 cm) possesses coarser sediments that likely indicate relatively enhanced dynamic conditions during deposition.

The excess ^{210}Pb profile (activity versus depth) for Core AC1 (Fig. 8b) indicates a two-segmented profile with a clear boundary

at 38 cm below the surface, corresponding to a transition of the dominant sediment fraction from sand to mud (Fig. 8a and b). Geochemical analysis of organic carbon confirmed that the lower segment can be explained by rapid fluvial sedimentation before abandonment, whereas the upper segment was dominated by sedimentation from marine sources due to tidal delivery after channel abandonment (Wu et al., 2020).

The data from Core AC1 suggests a transition of the sedimentary environment from a fluvial depositional setting to an estuary, with the former characterized by relatively coarse sandy deposits and the latter by mud. Therefore, the upper part of the core can be used to constrain the thickness of mud deposition since abandonment and the initiation of estuarine conditions and associated sediment infilling of the Qingshuigou channel.

4. Results and discussion

4.1. Channel landform after abandonment

As supported by the above analyses, the present model effectively simulates the infilling processes in the abandoned channel, particularly for parameters $p_1 = -0.087$, $p_2 = 0.584$, $a = 2.55 \times 10^{-10}$, and $i = 0.8$. The model produces a predicted sediment distribution pattern within the Qingshuigou channel after 20 years of filling (Fig. 9) based on parameter values including model unknown parameters (a, i, p_1, p_2) and environmental parameters including the sediment net flux, sediment density, distance, porosity, erosion rate, water depth, and time.

As shown in Fig. 9, the mud-flat depositional thickness ranges from 0.12 m to 0.81 m. The estuary was shortened to 6580 m since channel abandonment in 1996 as a consequence of severe shoreline retreat. Slope 1 was the main contributor to deposition, although the thickest part of the mud flat is located near the tidal channel. The model demonstrates that slope 2 has a significant impact on the disparity in sediment discharge between spring tide and overbank deposition. The model predicts that closer proximity to the tidal channel results in deposition of more sediment. The slope angle from the estuary to the landside declines, becoming steeper near the estuary and flattening landward.

The morphology observed today is not necessarily indicative of the filling patterns of the past two decades. Hence, to evaluate how depositional processes arose over the past 19 years, we examined the time-series results of the model. Fig. 10 shows a sediment deposition distribution map with five-year intervals. It is notable that estuary erosion caused a shortening of the mud flat over the modeled 19 years. Parameter m is the distance to the estuary, and parameter n

is the distance to the tidal channel, so it is convenient to explore the different influences of slopes 1 and 2 over the time series. In the first year, the shore-normal slope (slope 1) definitely controls deposition owing to its similarity to the mud flat (Fig. 10a). Levees started to form initially, and a deposition "hot spot" developed and moved landward with time. Subsequently, overbank processes (slope 2) began to play a more decisive role in influencing deposition (Fig. 10b–e). This indicates that deposition rates are higher than those for slope 1. It should be noted that we use the average deposition rate for slope 2, meaning that deposition from the tidal channel is assumed to be uniform.

To evaluate whether there is variation in the shore-normal tide deposition rate, sediment profiles are compared over the nineteen-year period of the model (Fig. 11a). Sediment thickness (η) increases over time; however, the incremental rate diminishes between 1996 and 2015. In the early stages, there is a relatively high rate, and landward deposition is thicker compared with that of the estuary. One year later, there is a 0.06 m accumulation landward, and after five years, accumulation increases to 0.13 m. The sedimentation rate declines over the last four years, totaling only a quarter of the value of the first five years and half the value of the first year. There is a clear increase in the slope angle, with the profile in 2015 being much steeper than that in 1996. These analyses indicate steady deposition onto the mud flat, with higher depositional rates landward.

It is important to note that the model operates within a defined time range. Abandoned channel mud flats have a continuous sediment source only within the water line, meaning that spring tide and overbank sources could not continue to contribute once the deposition thickness becomes greater than water depth. According to the model results, the thickest part of the mud flat is located near the tidal channel, meaning that it would be the earliest non-submerged area to become a supratidal zone without influence from the spring tide. After that, the remaining mud flat would be gradually isolated from the tidal channel, eventually forming a normal tidal flat. However, the abandoned channel body suffers from rapid shoreline retreat caused by strong ocean dynamics, shortening the channel and reducing the depositional area. The equilibrium state of the abandoned channel would primarily depend upon the in-channel depositional rate and the sediment supply from nearshore erosion.

4.2. Sensitivity to boundary conditions

All of the described results are for average and stable environmental boundary conditions. These parameters can vary, and so it is useful to test the model sensitivity. Since environmental conditions have a greater influence on slope 1, we focus on changes in profiles from estuary to land. The boundary conditions for slope 1 are described by Eq. (8) and include sediment flux (ΔUC_m), erosion rate (e) and water depth (H_0). Fig. 11b shows the result when sediment flux (ΔUC_m), erosion rate (e) and water depth (H_0) are halved.

The model result based on the original boundary conditions was defined as a standardization line for comparing variable environments. When sediment flux is reduced by half, maximum deposition changes from 27.4 cm to 20.7 cm (24.3% decline). Except for the proportion of sediments attributable to slope 2, the percentage decrease in slope 1 is 28.7% (Fig. 11b). This indicates that variation in sediment flux results in a nonproportional reduction in the deposition rate. Varying water depth results in a similar variation in deposition, resulting in a depositional thickness of 20.4 cm (25.4% decline). This indicates that the depositional model is slightly more sensitive to water depth. When the erosion rate is adjusted (slower channel shortening), the depositional thickness shows a slight increase to 28.0 cm (2.41% increase). Though halving the erosion rate produces a longer channel and a wider depositional area, it seems to have little influence on depositional processes within an abandoned channel.
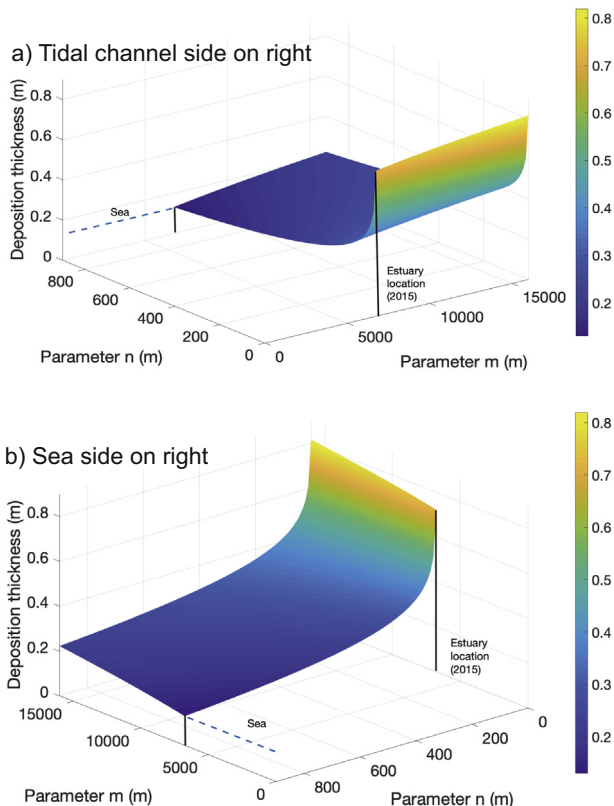
Fig. 9. Distribution map of in-channel deposition in 2015 based on model results. a) The tidal channel levee is on the right side; b) the sea is on the right side. The color bar indicates the deposit thickness range. Parameter m is the distance from the 1996 estuary and parameter n is the distance from the tidal channel. The black line marks the location of the 2015 estuary. The blue dashed line represents the offshore sea.
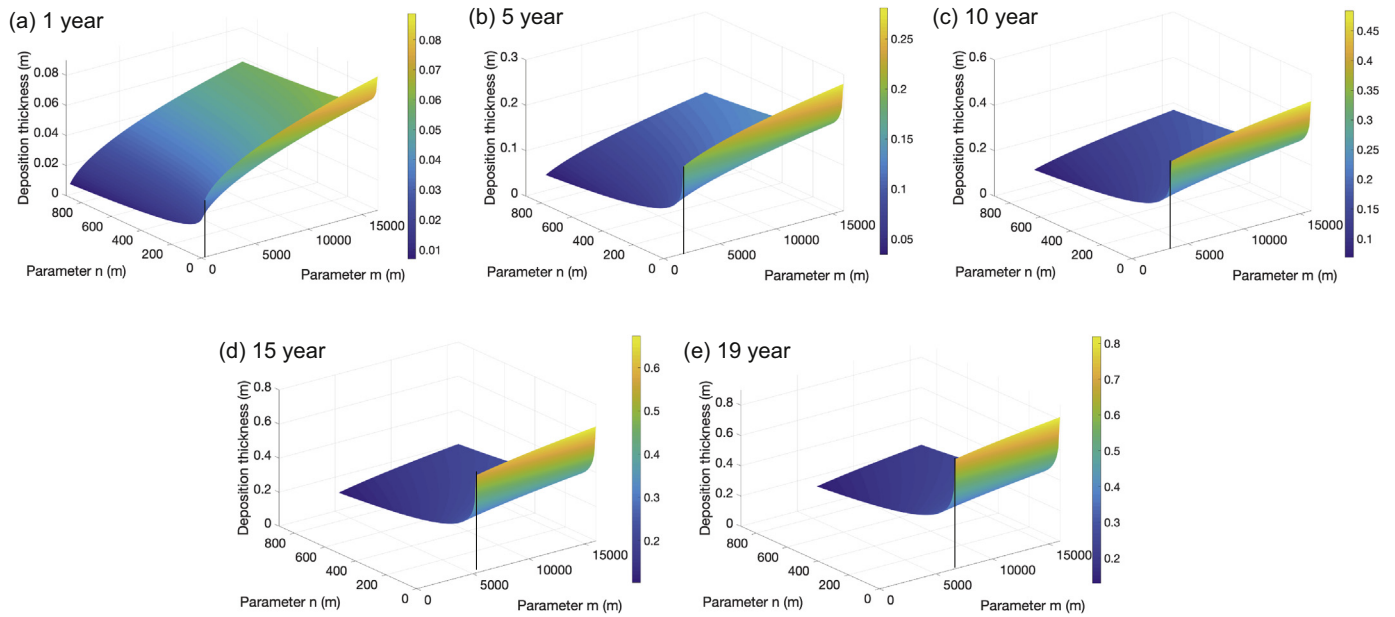
Fig. 10. Sediment deposition distribution map at different stages: a) 1 year, b) 5 years, c) 10 years, d) 15 years and e) 19 years, based on model results. The color bar indicates the deposition thickness range. Parameter *m* is the distance from the 1996 estuary and parameter *n* is the distance from the tidal channel. The black line marks the location of the estuary in 2015.

4.3. Infilling volume of sediment in the abandoned channel

Since deposition and lobe retreat via erosion are simultaneous processes in the abandoned channel, it is worthwhile to discuss how much sediment could be contributed to channel filling as a consequence of lobe erosion. The model results allow calculation of the deposition volume of sediment via integration of the in-channel depositional thickness and the depositional area inside the channel (Fig. 12).

Sediment volume contributed by shore-normal flow is the largest part of total deposition, while sediment carried by the shore-parallel flow process is incremental, thus indicating a similar solution: shore-parallel flow is a significant phenomenon in shaping mudflat morphology in the late stage (Fig. 2c). As with the dispositional rate, the total sediment volume filling the channel rapidly increases in the initial stage and maintains a net increase in subsequent years but with a decelerating rate. Sediment deposition for a shore-normal slope maintains a constant value, even though it shows a decreasing trend, with sediment from overbank sources similarly diminishing. Eventually, sediment volume contributed by a shore-normal slope is less than that of the previous year (Fig. 12). The trend of the reduction in sediment volume appears to be caused by the shorter estuary channel, leading to a shrinking of the mud flat and a decrease in the depositional area (Fig. 2c). Therefore, the existing sediment accumulation near the estuary may be eroded and removed.

4.4. Impacts of seasonal dynamics on mud flat evolution

As mentioned in the section on model parameters, suspended sediment concentrations in winter near the mouth of the Yellow River are ~18–28 times higher than those in summer, indicating a significant seasonal variation. Strong northerly or northwesterly winds prevail in winter and spring and are associated with enhanced wave actions and coastal currents, controlling sediment distribution and transport. Sediments in the Bohai Sea are evidently sensitive to monsoonal signals due to the shallow depth and an adequate terrestrial sediment supply. Furthermore, for the Yellow River, the main factor that considerably enhances sediment concentrations in the adjacent coastal region is the

occurrence of extreme winter storms (Yang et al., 2011; Wang et al., 2014; Zeng et al., 2015).

For abandoned distributary channels in the Yellow River delta, an evident seasonal influence affects sediment flux carried by spring tides and deposited on normal slopes onshore. Meanwhile, landforms and hydrodynamics are highly modulated by intense winter monsoons. Despite limitations of the field data that constrain the boundary conditions, the model supports the generalization that winter mode sediment flux lasts approximately a half year (winter-spring) and transitions to summer (summer-autumn) mode for the rest of the year, indicating that sediment mainly accumulates in the winter. As a potentially major sink of marine-sourced suspended sediment, abandoned channels play a greater role in winter as receivers of sediment.

4.5. Model implications for understanding tidal channels and mud flat evolution

As a composite land-ocean interface with multiple sediment sources and initial conditions that include a limited flat depositional area and specific submerged periods, abandoned channels differ importantly from general tidal flats and tidal channel environments. Maintaining an inherited morphological channel structure, the main bodies of abandoned channels can be viewed as large tidal flats restricted by identifiable levees, influenced by cross spring tides and resulting in shore-normal slopes (slope 1). Meanwhile, nearshore erosion induced by ocean dynamics provides a new overbank sediment source for mud flats, forming a shore-parallel slope (slope 2). This complex sedimentary environment distinguishes the contrasting morphological features of abandoned channels compared with those of broad coastal tidal flats. The new method we propose can be used to model abandoned deltaic channel geomorphology and deposition quantities regardless of the limitations imposed by residual channels. Furthermore, we suggest that it is important to investigate the landform evolution of tidal flats with finite boundaries, which are common in artificial coastal structures.

The model results suggest that the abandoned channel was filled with several million tons of sediment over the past 19 years (Fig. 12), forming a mud flat with a steeper frontier that flattened landward and
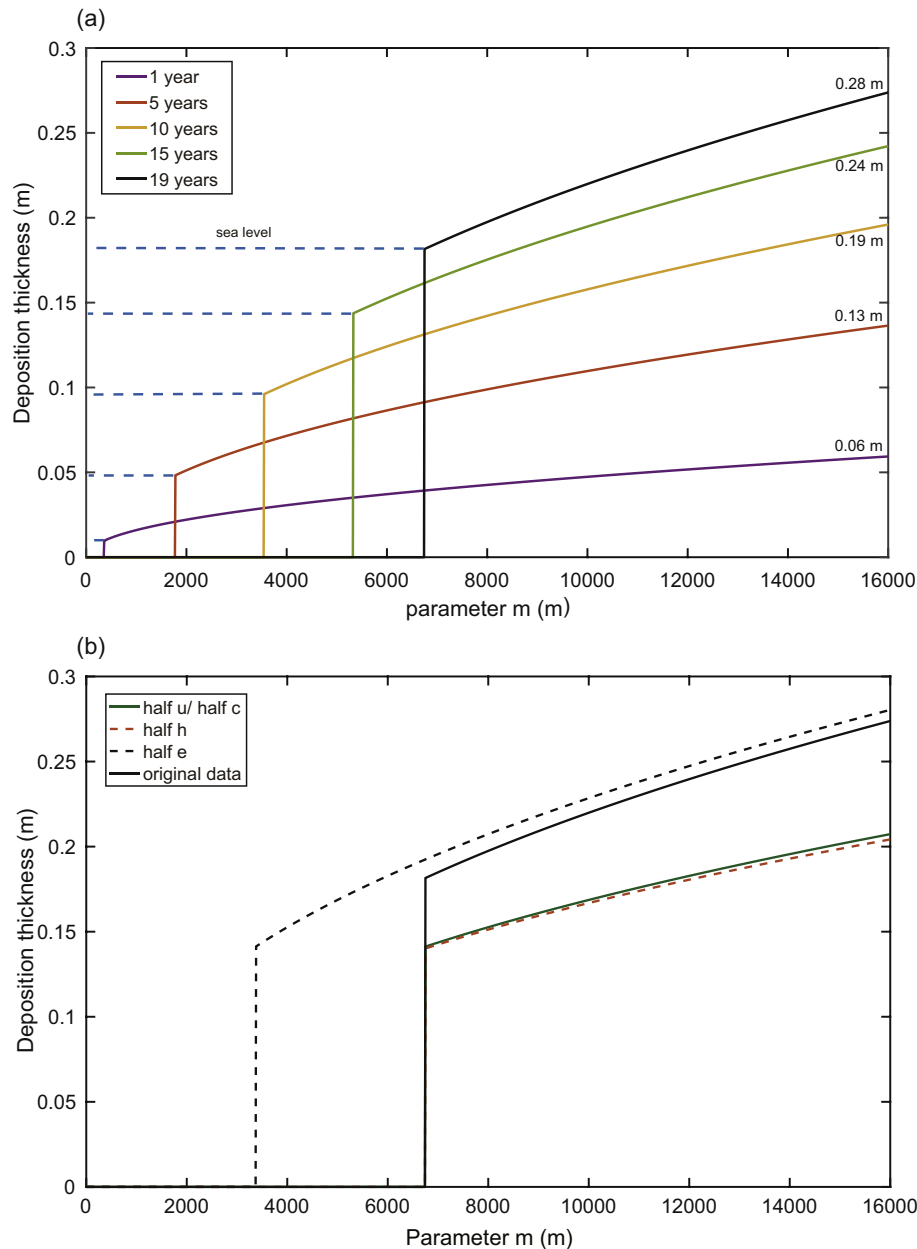
Fig. 11. a) Sediment deposition distribution profiles at 1 year, 5 years, 10 years, 15 years and 19 years after channel abandonment. Here, parameter $n = 500$. Dashed lines represent offshore sea level; b) sediment deposition constrained by different environmental boundary conditions, including changes in sediment flux (half current speed or half sediment concentration), water depth (half water depth), and erosion rate (half erosion rate). Here, parameter $n = 500$, and parameter $t = 19$ years.

with the tidal channel overbank levee being the thickest depocenter (Fig. 2c). It is noteworthy that the tidal channel, which is the secondary sediment source, provides sustained overbank deposition that may predominate the morphological evolution of mud flat landforms in the late stage. The role of in-channel accumulation as a new sediment sink potentially plays a critical role in balancing the sediment budget of the Yellow River delta.

5. Conclusion

As composite landforms at the ocean interface, the morphological evolution of abandoned channels with multiple sediment sources differs importantly from that of general tidal flats. The main body of the abandoned channel is influenced by the morphological structure of the antecedent channel, with identifiable levees that constrain tidal flows and result in a large tidal flat with a shore-normal slope and a

shore-parallel slope that provides a sediment source for mud flat development.

A quantitative model is established for examination of the geomorphological evolution of an abandoned deltaic channel. The model results indicate that an abandoned channel is a site for sediment accumulation, forming a mud flat with a steep front that flattens landward, while tidal channel overbank levees form the thickest depocenter. It is noteworthy that tidal channels, as secondary sediment sources, provide sustained overbank deposition and primarily control mudflat landforms in the late stages. The variation in sediment flux results in a nonproportional reduction in the deposition rate, while varying water depth results in similar but slightly more sensitive variation. Halving the erosion rate produces a longer channel and a wider depositional area, though there is little influence on depositional processes within an abandoned channel. Owing to the gradual increase in slope, the depositional rate in the abandoned channel decreases with time, resulting in a decelerating rate
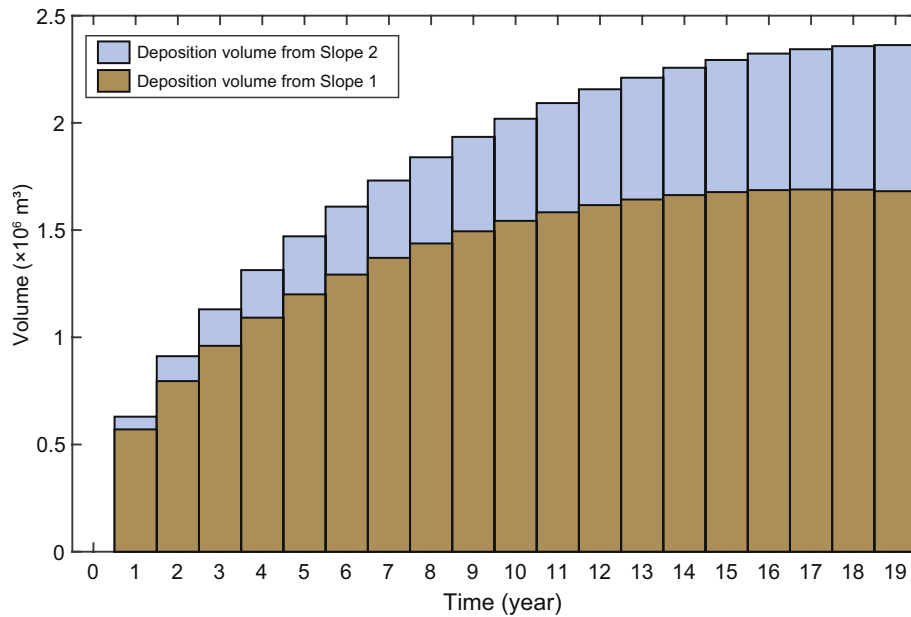
Fig. 12. Model-derived infilling volume of sediment from 1996 to 2015. The volume from slope 1 indicates sediment deposition by cross spring tides and that from slope 2 is overbank deposition.

of infilling sediment volume, while strong winter monsoons and extreme storms dominate sediment concentration and in-channel deposition. The abandoned fluvial-deltaic distributary channel acts as a new sediment sink that potentially plays a critical role in the sediment budget of the Yellow River delta. Our new approach can add significantly to the understanding of the infilling process of abandoned distributary channels in large river deltas worldwide.

Declaration of competing interest

The authors declare that they have no known competing financial interests or personal relationships that could have appeared to influence the work reported in this paper.

Acknowledgements

References

Belliard, J.P., Toffolon, M., Carniello, L., D'Alpaos, A., 2015. An ecogeomorphic model of tidal channel initiation and elaboration in progressive marsh accretional contexts. J. Geophys. Res. Earth Surf. 120 (6), 1040–1064. https://doi.org/10.1002/2015JF003445.

Bi, N., Yang, Z., Wang, H., Hu, B., Ji, Y., 2010. Sediment dispersion pattern off the present Huanghe (Yellow River) subdelta and its dynamic mechanism during normal river discharge period. Estuar. Coast. Shelf Sci. 86 (3), 352–362. https://doi.org/10.1016/j.ecss.2009.06.005.

Carlson, B., Nittrouer, J., Moodie, A.J., Kineke, G.C., Kumpf, L.L., Ma, H., Parsons, D.R., Wang, H., 2020. Infilling abandoned deltaic channels through tidal sedimentation: a case study from the Huanghe (Yellow River) delta, China. J. Geophys. Res. Earth Surf. https://doi.org/10.1029/2019JF005254 e2019JF005254.

Chatanantavet, P., Lamb, M.P., Nittrouer, J.A., 2012. Backwater controls of avulsion location on deltas. Geophys. Res. Lett. 39 (1). https://doi.org/10.1029/2011GL050197 L01402.

Fagherazzi, S., Kirwan, M.L., Mudd, S.M., Guntenspergen, G.R., Temmerman, S., D'Alpaos, A., Clough, J., 2012. Numerical models of salt marsh evolution: Ecological, geomorphic, and climatic factors. Rev. Geophys. 50 (1). https://doi.org/10.1029/2011RG000359 RG1002.

Frazier, D.E., 1967. Recent deltaic deposits of the Mississippi River: their development and chronology. Gulf Coast Association of Geological Societies Transactions. 17, pp. 287–315.

Friedrichs, C., Aubrey, D., 1996. Uniform bottom shear stress and equilibrium hyposometry of intertidal flats. In: Parttiaratchi, C. (Ed.), Mixing in Estuaries and Coastal Seas (Coastal and Estuarine Studies: 50). American Geophysical Union, Washington DC, pp. 405–429. https://doi.org/10.1029/CE050p0405.

Friedrichs, C.T., 2011. Tidal flat morphodynamics: a synthesis. In: Flemming, B.W., Hansom, J.D. (Eds.), Treatise on Estuarine and Coastal Science: Sedimentology and Geology. Elsevier, pp. 137–170. https://doi.org/10.1016/B978-0-12-374711-2.00307-7.

Hsu, T.J., Chen, S.N., Ogston, A.S., 2013. The landward and seaward mechanisms of fine-sediment transport across intertidal flats in the shallow-water region—a numerical investigation. Cont. Shelf Res. 60, S85–S98. https://doi.org/10.1016/j.csr.2012.02.003.

Hu, Z., Wang, Z.B., Zitman, T.J., Stive, M.J., Bouma, T.J., 2015. Predicting long-term and short-term tidal flat morphodynamics using a dynamic equilibrium theory. J. Geophys. Res. Earth Surf. 120 (9), 1803–1823. https://doi.org/10.1002/2015JF003486.

Hu, Z., Van Der Wal, D., Cai, H., Van Belzen, J., Bouma, T.J., 2018. Dynamic equilibrium behaviour observed on two contrasting tidal flats from daily monitoring of bed-level changes. Geomorphology 311, 114–126. https://doi.org/10.1016/j.geomorph.2018.03.025.

Jia, Y., Shan, H., 2011. Sediment Dynamics and Geologic Hazards in the Estuary of Yellow River. Science Press, Beijing.

Kearney, W.S., Fagherazzi, S., 2016. Salt marsh vegetation promotes efficient tidal channel networks. Nat. Commun. 7, 12287. https://doi.org/10.1038/ncomms12287.

Le Hir, P., Roberts, W., Cazaillet, O., Christie, M., Bassoullet, P., Bacher, C., 2000. Characterization of intertidal flat hydrodynamics. Cont. Shelf Res. 20 (12–13), 1433–1459. https://doi.org/10.1016/S0278-4343(00)00031-5.

Lee, H.J., Jo, H.R., Chu, Y.S., Bahk, K.S., 2004. Sediment transport on macrotidal flats in Garolim Bay, west coast of Korea: significance of wind waves and asymmetry of tidal currents. Cont. Shelf Res. 24 (7–8), 821–832. https://doi.org/10.1016/j.csr.2004.01.005.

Lee, S.-C., Mehta, A.J., 1997. Problems in characterizing dynamics of mud shore profiles. J. Hydraul. Eng. 123 (4), 351–361. https://doi.org/10.1061/(ASCE)0733-9429(1997)123:4(351).

Ma, H., Nittrouer, J.A., Naito, K., Fu, X., Zhang, Y., Moodie, A.J., Parker, G., 2017. The exceptional sediment load of fine-grained dispersal systems: example of the Yellow River, China. Sci. Adv. 3 (5). https://doi.org/10.1126/sciadv.1603114 e1603114.

Mariotti, G., Fagherazzi, S., 2010. A numerical model for the coupled long-term evolution of salt marshes and tidal flats. J. Geophys. Res. Earth Surf. 115, F01004. https://doi.org/10.1029/2009JF001326.

Mariotti, G., Fagherazzi, S., 2013. A two-point dynamic model for the coupled evolution of channels and tidal flats. J. Geophys. Res. Earth Surf. 118 (3), 1387–1399. https://doi.org/10.1002/jgrf.20070.

Milliman, J.D., Meade, R.H., 1983. World-wide delivery of river sediment to the oceans. The Journal of Geology 91 (1), 1–21. https://doi.org/10.1086/628741.

Milliman, J.D., Syvitski, J.P., 1992. Geomorphic/tectonic control of sediment discharge to the ocean: the importance of small mountainous rivers. J. Geol. 100 (5), 525–544. https://doi.org/10.1086/629606.

Nienhuis, J.H., Ashton, A.D., Roos, P.C., Hulscher, S.J., Giosan, L, 2013. Wave reworking of abandoned deltas. Geophys. Res. Lett. 40 (22), 5899–5903. https://doi.org/10.1002/2013GL058231.

Pang, J., Si, S., 1979. The estuary changes of Huanghe River I: changes in modern time. Oceanologia Et Limnologia Sinica 2, 136–141.

Penland, S., Boyd, R., Suter, J.R., 1988. Transgressive depositional systems of the Mississippi Delta plain; a model for barrier shoreline and shelf sand development. J. Sediment. Res. 58 (6), 932–949. https://doi.org/10.1306/212F8EC2-2B24-11D7-8648000102C1865D.

Postma, H., 1961. Transport and accumulation of suspended matter in the Dutch Wadden Sea. Neth. J. Sea Res. 1 (1–2), 148–190. https://doi.org/10.1016/0077-7579(61)90004-7.

Pritchard, D., Hogg, A.J., Roberts, W., 2002. Morphological modelling of intertidal mudflats: the role of cross-shore tidal currents. Cont. Shelf Res. 22 (11—13), 1887–1895. https://doi.org/10.1016/S0278-4343(02)00044-4.

Roberts, W., Le Hir, P., Whitehouse, R., 2000. Investigation using simple mathematical models of the effect of tidal currents and waves on the profile shape of intertidal mudflats. Cont. Shelf Res. 20 (10—11), 1079–1097. https://doi.org/10.1016/S0278-4343(00)00013-3.

Straaten, L.M.J.U., Kuenen, P.H.H., 1958. Tidal action as a cause of clay accumulation. J. Sediment. Res. 28 (4), 406–413. https://doi.org/10.1306/74D70826-2B21-11D7-8648000102C1865D.

Wang, A., Wang, H., Bi, N., Wu, X., 2016. Sediment transport and dispersal pattern from the Bohai Sea to the Yellow Sea. J. Coast. Res. SI 74, 104–116. https://doi.org/10.2112/SI74-010.1.

Wang, H., Yang, Z., Li, G., Jiang, W., 2006. Wave climate modeling on the abandoned Huanghe (Yellow River) Delta lobe and related deltaic erosion. J. Coast. Res. 224, 906–918. https://doi.org/10.2112/03-0081.1.

Wang, H., Yang, Z., Li, Y., Guo, Z., Sun, X., Wang, Y., 2007. Dispersal pattern of suspended sediment in the shear frontal zone off the Huanghe (Yellow River) mouth. Cont. Shelf Res. 27 (6), 854–871. https://doi.org/10.1016/j.csr.2006.12.002.

Wang, H., Wang, A., Bi, N., Zeng, X., Xiao, H., 2014. Seasonal distribution of suspended sediment in the Bohai Sea, China. Cont. Shelf Res. 90, 17–32. https://doi.org/10.1016/j.csr.2014.03.006.

Wang, H., Wu, X., Bi, N., Li, S., Yuan, P., Wang, A., Syvitski, J.P.M., Saito, Y., Yang, Z., Liu, S., Nittrouer, J., 2017. Impacts of the dam-orientated water-sediment regulation scheme on the lower reaches and delta of the Yellow River (Huanghe): a review. Glob. Planet. Chang. 157, 93–113. https://doi.org/10.1016/j.gloplacha.2017.08.005.

Wu, X., Wang, H., Bi, N., Nittrouer, J.A., Xu, J., Cong, S., Li, Z., 2020. Evolution of a tide-dominated abandoned channel: a case of the abandoned Qingshuigou course, Yellow River. Mar. Geol. 422, 106116. https://doi.org/10.1016/j.margeo.2020.106116.

Xu, F., Coco, G., Tao, J., Zhou, Z., Zhang, C., Lanzoni, S., D'Alpaos, A., 2019. On the morphodynamic equilibrium of a short tidal channel. J. Geophys. Res. Earth Surf. 124 (2), 639–665. https://doi.org/10.1029/2018JF004952.

Xue, C., 1993. Historical changes in the Yellow River delta, China. Mar. Geol. 113 (3), 321–330. https://doi.org/10.1016/0025-3227(93)90025-Q.

Yang, Z., Ji, Y., Bi, N., Lei, K., Wang, H., 2011. Sediment transport off the Huanghe (Yellow River) delta and in the adjacent Bohai Sea in winter and seasonal comparison. Estuar. Coast. Shelf Sci. 93 (3), 173–181. https://doi.org/10.1016/j.ecss.2010.06.005.

Zeng, X., He, R., Xue, Z., Wang, H., Wang, Y., Yao, Z., Warrillow, J., 2015. River-derived sediment suspension and transport in the Bohai, Yellow, and East China Seas: A preliminary modeling study. Cont. Shelf Res. 111, 112–125. https://doi.org/10.1016/j.csr.2015.08.015.

Zhou, L., Liu, J., Saito, Y., Zhang, Z., Chu, H., Hu, G., 2014. Coastal erosion as a major sediment supplier to continental shelves: example from the abandoned Old Huanghe (Yellow River) delta. Cont. Shelf Res. 82, 43–59. https://doi.org/10.1016/j.csr.2014.03.015.